Article

Neuron

Distinct Subthreshold Mechanisms Underlying Rate-Coding Principles in Primate Auditory Cortex

Highlights

- We developed a novel intracellular recording technique for awake primates
- A1 neurons show unique spiking and subthreshold responses to time-varying sounds
- Two types of rate-coding A1 neurons exhibited distinct subthreshold responses
- Computational model provides mechanistic insights to diverse temporal coding schemes

Authors

Lixia Gao, Kevin Kostlan, Yunyan Wang, Xiaoqin Wang

Correspondence

xiaoqin.wang@jhu.edu

In Brief

Using a novel intracellular recording technique developed for studying awake primate brain, Gao et al. found distinct subthreshold responses underlying diverse temporal coding schemes in auditory cortex.

Gao et al., 2016, Neuron *91*, 1–15
August 17, 2016
http://dx.doi.org/10.1016/j.neuron.2016.07.004

CellPress

Please cite this article in press as: Gao et al., Distinct Subthreshold Mechanisms Underlying Rate-Coding Principles in Primate Auditory Cortex, Neuron (2016), http://dx.doi.org/10.1016/j.neuron.2016.07.004

Neuron
Article

Distinct Subthreshold Mechanisms Underlying Rate-Coding Principles in Primate Auditory Cortex

Lixia Gao,[1] Kevin Kostlan,[1] Yunyan Wang,[1] and Xiaoqin Wang[1,*]
[1]Laboratory of Auditory Neurophysiology, Department of Biomedical Engineering, Johns Hopkins University School of Medicine, Baltimore, MD 21025, USA
*Correspondence: xiaoqin.wang@jhu.edu
http://dx.doi.org/10.1016/j.neuron.2016.07.004

SUMMARY

A key computational principle for encoding time-varying signals in auditory and somatosensory cortices of monkeys is the opponent model of rate coding by two distinct populations of neurons. However, the subthreshold mechanisms that give rise to this computation have not been revealed. Because the rate-coding neurons are only observed in awake conditions, it is especially challenging to probe their underlying cellular mechanisms. Using a novel intracellular recording technique that we developed in awake marmosets, we found that the two types of rate-coding neurons in auditory cortex exhibited distinct subthreshold responses. While the positive-monotonic neurons (monotonically increasing firing rate with increasing stimulus repetition frequency) displayed sustained depolarization at high repetition frequency, the negative-monotonic neurons (opposite trend) instead exhibited hyperpolarization at high repetition frequency but sustained depolarization at low repetition frequency. The combination of excitatory and inhibitory subthreshold events allows the cortex to represent time-varying signals through these two opponent neuronal populations.

INTRODUCTION

In sound processing, time is an essential dimension of auditory signals. Temporal information is especially crucial for perceiving and discriminating communication sounds such as human speech (Moore, 2003; Rosen, 1992) and animal vocalizations (Singh and Theunissen, 2003), as well as musical melodies and rhythms (Peretz and Zatorre, 2005). How the brain processes temporal information remains a core question in auditory research. At processing stations along the ascending auditory pathway, beginning at the auditory nerve, neurons' ability to synchronize to time-varying stimuli progressively decreases such that by the time the signal reaches the auditory cortex, the synchronization rate is well below 100 Hz, too slow to encode critical features in speech and music (Joris et al., 2004; Wang, 2007). The drastic reduction of firing synchronization in auditory cortex had puzzled auditory neurophysiologists for a long time until experiments were conducted in awake animals where an alternative rate-coding scheme was discovered (Bendor and Wang, 2007; Lu et al., 2001b; Wang et al., 2008). A marked feature of neural responses in auditory cortex in awake states is the pronounced sustained firing (Wang et al., 2005), in sharp contrast to transient firing observed in anesthetized preparations (Heil, 1997; Phillips, 1985). It has been suggested that auditory cortex uses a combination of stimulus-synchronized and non-synchronized responses to encode the temporal information of sounds, with the non-synchronized responses encoding temporal features that vary too quickly to be captured by stimulus-synchronized firing (Bendor and Wang, 2007; Lu et al., 2001b; Wang et al., 2008).

This notion of "non-synchronized response" in auditory cortex, i.e., neurons having increasing firing rate with increasing stimulus repetition frequency, was first observed in awake marmosets (Lu et al., 2001b) and later confirmed by Gao and Wehr (2015) in awake rats. However, the non-synchronized response alone as proposed in these previous studies is not sufficient for rate encoding because firing rate is also influenced by other parameters such as sound level and thus does not uniquely represent stimulus repetition frequency. Bendor and Wang (2007) proposed an opponent model to solve this problem in auditory cortex by having two types of non-synchronized responses with opposite slopes as a function of increasing stimulus repetition frequency (Bendor and Wang, 2007). These two distinct types of neurons are respectively referred to as "positive monotonic" (nSync+), which shows increasing firing rate with increasing repetition frequency, and "negative monotonic" (nSync−), which shows increasing firing rate with decreasing repetition frequency. A similar rate-coding scheme was proposed by Romo and colleagues to encode the frequency of vibrotactile stimuli by somatosensory cortex of monkeys (Romo and Salinas, 2003; Salinas et al., 2000). While the opponent rate-coding model is supported by evidence from extracellular recording experiments, it has remained unclear which cellular mechanisms give rise to such response properties. Computationally, the positive-monotonic response can be modeled by temporal integration of synchronized (Gao and Wehr, 2015) or successive excitatory inputs (Bendor, 2015; Gao and Wehr, 2015; Rabang and Bartlett, 2011). However, the negative-monotonic response is counterintuitive to the commonly used temporal integration model. To date, no study has investigated the subthreshold activities underlying these two types of non-synchronized responses in auditory or somatosensory cortex. The

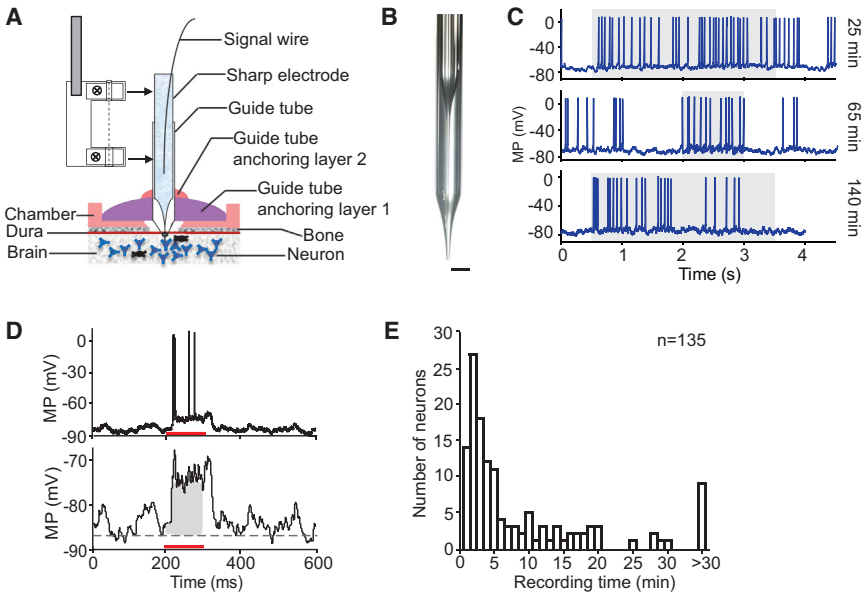

Figure 1. Co-axial Guide Tube Protected Sharp Electrode Recording Method

(A) Schematic diagram of guide-tube-anchored sharp electrode recording method. Left top (gray color), side view of the custom-made electrode holder. The co-axial grooves of the holder were used to hold the sharp electrode (small groove) and guide tube (large groove), respectively, and also functioned as a guide to align the two electrodes together. Two screws were used to fasten the recording electrode and guide tube. Right bottom (purple and pink colors), side view of the arrangement of the guide tube anchor.

(B) Photograph of the recording electrode and guide tube assembly after they were loaded and fastened into the electrode holder. Scale bar, 1 mm.

(C) Example traces from a cortical neuron held for 160 min at the beginning (top, at 25 min), middle (middle, at 65 min), and end of the recording (bottom, at 140 min). Gray shaded area indicates periods of sound stimulation (top, pure tone; middle, sAM tone; bottom, white broad-band noise). x axis label applied to all panels.

(D) Top, an example of auditory response elicited by a tone. Bottom, the subthreshold response of the same trial after the spikes were removed by line interpolation method (note the different voltage scales). The dashed gray line is the baseline MP. Stimulus duration is indicated by the red bar. The area of subthreshold response is shown by the gray shaded area.

(E) Histogram of the duration of intracellular recordings, binned to the nearest minute.

present study made an effort to provide a cellular explanation of the opponent rate-coding model in the cortex of awake nonhuman primates.

In vivo intracellular recording is a powerful tool for studying the cellular mechanisms underlying neural firing patterns observed by extracellular recording, but has traditionally been carried out in anesthetized animals since stability is more easily maintained in such preparations (Gao et al., 2009; Steriade et al., 1993). However, any commonly used intracellular recording techniques have been developed for rodents and small animals, where the yield per animal is quite low (Chorev et al., 2009). It has remained a formidable challenge to conduct reliable and high-yield intracellular recording from awake nonhuman primates (Long and Lee, 2012). Because the non-synchronized responses in auditory cortex cannot be observed under anesthesia (Bendor and Wang, 2007; Lu et al., 2001b; Wang et al., 2008), it is necessary to study their cellular mechanisms in awake animals. In the present study, we have developed a novel intracellular recording technique to examine these questions in a large number of intracellularly recorded neurons from the auditory cortex of awake common marmoset (*Callithrix jacchus*). Marmosets are a highly vocal and social nonhuman primate species (Agamaite et al., 2015; Miller et al., 2016). They have a similar hearing range (Osmanski and Wang, 2011) and pitch perception behaviors (Song et al., 2016) to humans and a cortical organization similar to other nonhuman primates (Aitkin et al., 1986; de la Mothe et al., 2006; Bendor and Wang, 2008). They have a relatively flat and easily accessible auditory cortex (Aitkin et al., 1986; Wang, 2000) that is well suited for intracellular recordings. Using this technique, we have investigated the cellular mechanisms underlying the rate coding by the two distinct populations of neurons in marmoset auditory cortex. Our findings provide valuable insights into the functions of auditory cortex neurons without the effect of anesthetics. The findings described in this work will advance our understanding of the mechanisms underlying temporal information processing in the primate auditory cortex.

RESULTS

A Novel Approach for Intracellular Recording from Auditory Cortex of Awake Marmoset

Few intracellular studies have been conducted in awake nonhuman primates due to technical challenges such as mechanical instability from animal movements, brain pulsations, and the difficulty for electrode insertion through intact dura. The latter is important since dura removal would reduce recording stability and also increase the risk of infection in a chronic preparation. In the current study, we developed a co-axial guide tube and sharp electrode assembly to allow repeated intracellular recordings from the auditory cortex of awake marmosets (see Experimental Procedures; Figures 1A and 1B). Using this technique, we were able to perform intracellular recordings stably and reliably from the primary auditory cortex (A1) of awake marmosets over many sessions and obtain a much larger number of intracellularly studied neurons per animal than most previous studies (Figure 1C). The duration of intracellular recordings from individual neurons varied from a few minutes to more than 1 hr (11.3 ± 21.5 min, n = 135; Figure 1E). As the auditory responses usually exhibited sustained depolarization instead of monosynaptic postsynaptic potential in awake A1 (Figure 1D, top), the magnitude of the subthreshold response was measured by the area of the depolarization in the stimulus window instead of response amplitude (Figure 1D, bottom). The development of this novel intracellular recording technique

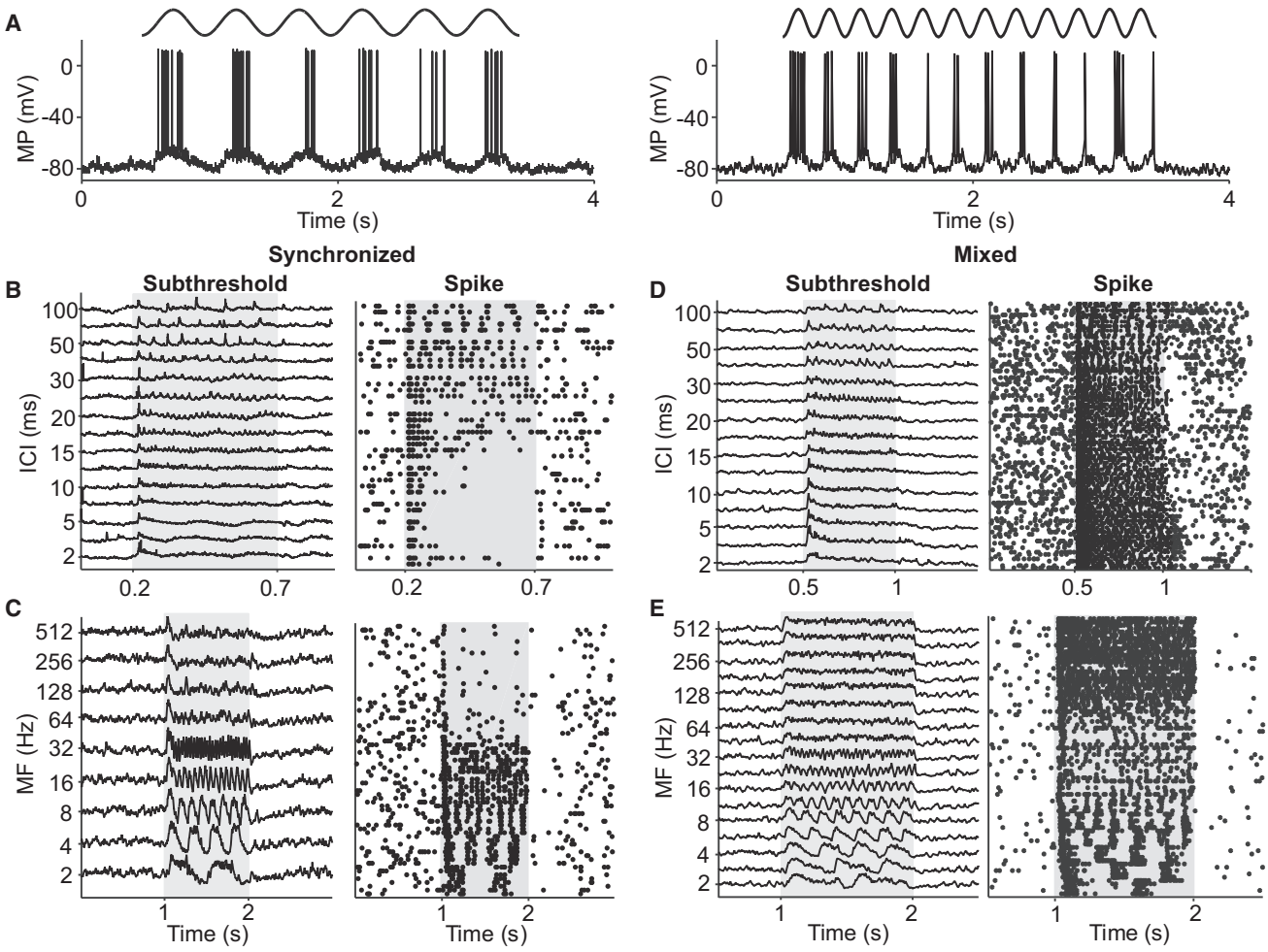

Figure 2. Periodic Depolarization Underlying Synchronized Discharge

(A) Two example trials showing the synchronized responses recorded intracellularly from a representative A1 neuron presented with sAM tone with MF at 2 Hz (left) and 4 Hz (right). The envelope of the sAM tone is represented above each panel.

(B–E) Synchronized (B and C) and mixed (D and E) responses elicited either by Gaussian click train with varying ICI (B and D) or sAM tone with varying MF (C and E) for four representative neurons. For each panel, the averaged subthreshold responses from five trials at each sound stimulation (left) and raster plot of discharge (right). Gray shaded area indicates the time periods of acoustic stimulation. See also Figure S1.

is crucial to tackling scientific questions of this work. We recorded both the membrane potential (MP) dynamics and spiking activities from 70 neurons in A1 from four hemispheres of three awake marmosets in response to Gaussian click trains with varying inter-click intervals (ICIs) (Lu et al., 2001b) or sinusoidal amplitude modulations (sAMs) with varying modulation frequency (MF) (Liang et al., 2002).

Periodic Depolarization Underlies Synchronized Discharges in A1 and Exhibits Faster Entrainment to Stimulus Repetition Frequency than Spiking Activity

A substantial number of A1 neurons in awake marmosets exhibit stimulus-synchronized responses (referred to as Sync neurons) to periodic stimuli at slow repetition frequency (Lu et al., 2001b; Wang et al., 2008). Exemplar A1 neurons with synchronized responses shown in Figure 2 exhibited precisely synchronized discharges at long ICIs (Figure 2B) or low MFs (Figure 2C), and their responses were suppressed at short ICIs or high MFs. For these neurons (18 of 70 neurons), their MP exhibited entrainment to the stimulus periodicity with spikes generated at the peaks of the periodic depolarization (Figure 2A). This consequently led to phase-locked discharge patterns to low repetition frequency. A smaller set of these neurons (9 of 70 neurons) exhibited mixed responses, with synchronized discharge at long ICIs (Figure 2D) or low MFs (Figure 2E) and increased sustained firing at short ICIs or high MFs. In this case, periodic depolarization underlies synchronized discharge, whereas sustained depolarization underlies sustained firing (Figures 2D and 2E).

Extracellular recording studies showed that medial geniculate body (MGB) neurons were able to synchronize to higher repetition frequency than A1 neurons (Creutzfeldt et al., 1980; Wang et al., 2008). As thalamocortical projections are the major excitatory inputs to A1 neurons, we would like to know whether subthreshold responses of A1 neurons are able to follow faster

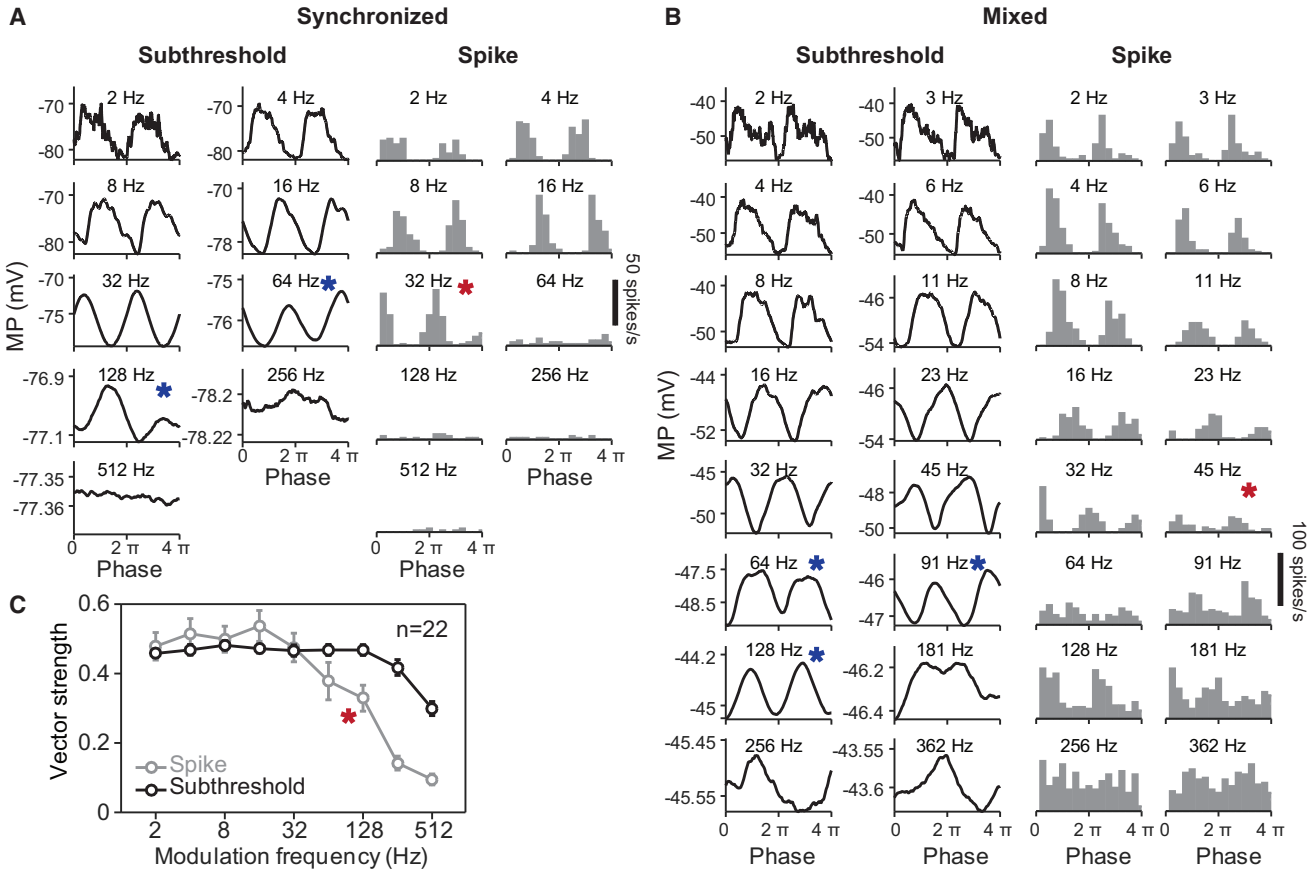

Figure 3. Periodicity of Subthreshold and Spiking Responses for Synchronized and Mixed Neurons

(A and B) Cycle-averaged histograms of subthreshold (left, black) and spiking (right, gray) responses for two example neurons shown in Figure 2, a synchronized neuron (A) and a Mixed neuron (B). Two complete stimulus cycles (0–4π) are shown. A median filter was used to remove spikes to obtain the subthreshold response. The calculated synchronization boundary of firing for each neuron is indicated by a red asterisk. Blue asterisks indicate periodic MP fluctuations for MFs above the synchronization boundary. Scale bar in cycle-averaged histograms of spiking responses (right panel) applies to all subplots.

(C) Mean VS of firing (gray) and that of subthreshold responses (black) plotted against MF for neurons with Sync and Mixed responses (n = 22; stimuli, sAM tone). The mean synchronization boundary of firing is indicated by the red asterisk. Error bars show SEM. See also Figure S2.

time-varying stimuli than the spiking response. Our intracellular recordings showed that subthreshold responses in A1 neurons exhibited periodic MP fluctuations even when spiking activities could no longer follow repetitive stimuli (Figure S1A, available online). To further compare the synchrony between the MP and spiking activity recorded from the same A1 neuron, we used vector strength (VS) and Rayleigh statistics (Lu and Wang, 2000; Mardia and Jupp, 2000) to quantify the synchronization of spiking responses for both synchronized (Figures S1B and S1C) and mixed responses (Figures S1D and S1E). The shortest ICI or highest MF to which a neuron showed significant synchronized firing for all longer ICIs or lower MFs was defined as the synchronization boundary (see Experimental Procedures). Next, we computed cycle-averaged histograms of the MP and corresponding spiking responses for these neurons. Both the MP fluctuations and firing rate showed clear periodicity at long ICIs (Figure S2) or low MFs (Figures 3A and 3B). However, above the synchronization boundaries of the spiking responses (marked by red asterisks), the MP still showed clear periodicity (marked by blue asterisks). We also calculated the VS of the MP (see Experimental Procedures) and compared it with that of spiking activity. Population analysis showed the VS of the MP was higher than that of spiking activity above the mean synchronization boundary of spiking activity (Figure 3C; $p < 0.001$), which indicated that the MP was entrained to higher stimulus repetition frequency than spiking activity in A1 neurons.

Distinct Subthreshold Mechanisms for Two Types of Non-synchronized Firing in A1

It was previously demonstrated that two subpopulations of non-synchronized A1 neurons (nSync+ and nSync−) in awake marmosets displayed increasing firing rate in response to increasing or decreasing stimulus repetition frequency, respectively (Bendor and Wang, 2007; Lu et al., 2001b). In our study, we recorded from both nSync+ (13 of 70 neurons) and nSync− (12 of 70 neurons) neurons in response to Gaussian click or sAM tone in A1 of awake marmosets. The neurons with nSync+ responses displayed sustained firing throughout the stimulus

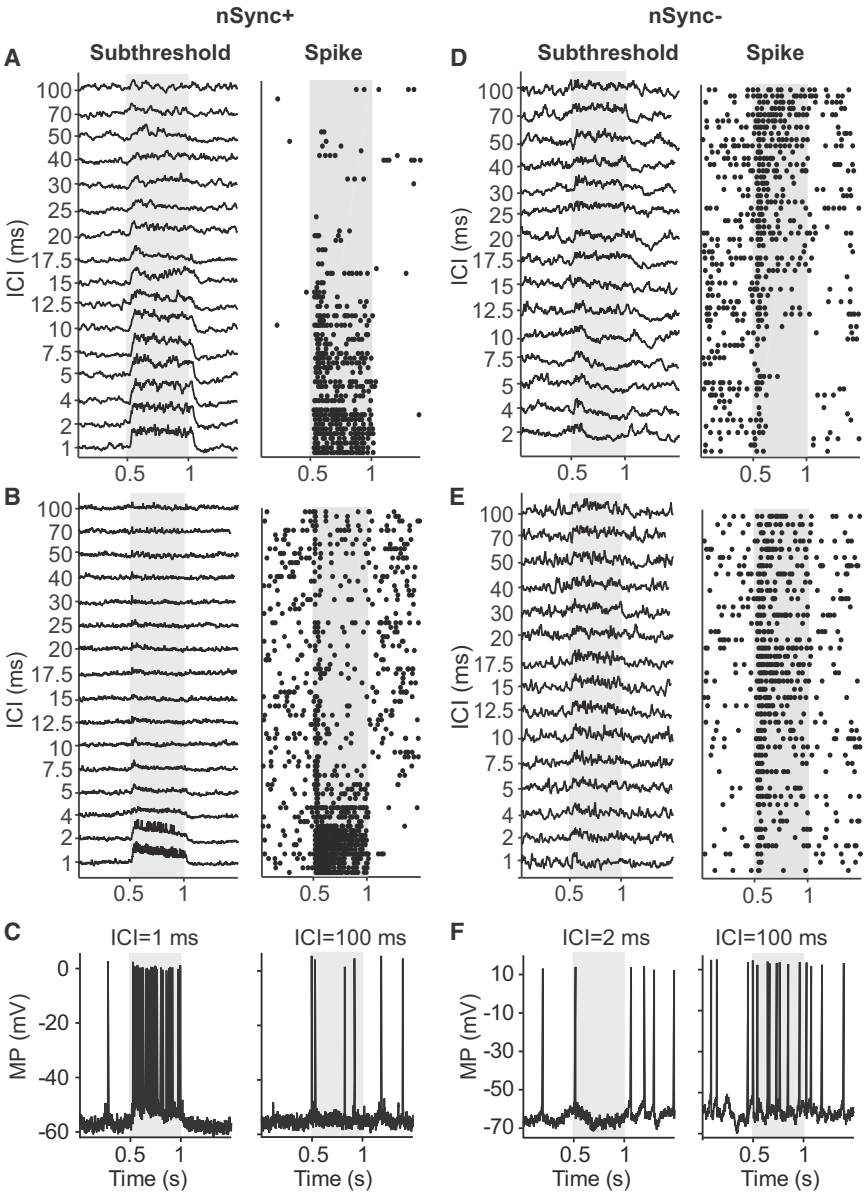

Figure 4. Sustained Depolarization Underlying nSync+ Response and Hyperpolarization Underlying nSync– Response

(A, B, D, and E) Examples of nSync+ (A and B) and nSync− (D and E) responses to click train from four representative neurons of A1. Left, mean subthreshold responses of five repetitions at each ICI. Right, raster plot of corresponding discharge.

(C and F) Example traces from nSync+ (C, from B) and nSync− (F, from D) responses at short and long ICIs, respectively. Stimulus duration is indicated by the gray shaded area in all figures. See also Figures S3A–S3D.

duration and pronounced sustained depolarization in the MP at short ICIs, as shown by two representative neurons in Figures 4A–4C. Their firing was not synchronized to the stimulus, as evidenced by Rayleigh statistics values below the significance level (13.8, $p < 0.001$) at ICIs <100 ms (Figures S3A and S3C). Both the firing rate and magnitude of depolarization of these nSync+ neurons increased with decreasing ICIs (Figures 5A and 5B). All nSync+ neurons showed significantly negative regression slope values when firing rate and depolarization were plotted against ICI (Figures 5E–5G, left panels).

In contrast, neurons with nSync− responses exhibited increased firing with increasing ICI (Figures 4D and 4E), but lacked significant synchronization to stimulus periodicity even at long ICIs (Figures S3B and S3D), which is consistent with previous extracellular recording studies in awake marmosets (Bendor and Wang, 2007). Interestingly, at short ICIs, nSync− neurons showed suppressed firing after the onset response and their MP exhibited hyperpolarization (Figures 4D–4F), as compared to the sustained depolarization exhibited by nSync+ neurons at short ICIs (Figures 4A–4C). In contrast to Sync and mixed neurons, nSync− neurons showed sustained rather than transient depolarization in MP at long ICIs (Figures 4D–4F versus Figure 2). For nSync− neurons, as the ICI changed from short to long, the magnitude of hyperpolarization decreased, whereas the magnitude of depolarization increased (Figures 4D and 4E). The sustained depolarization throughout stimulus duration at long ICIs gave rise to the sustained firing with increasing ICIs in nSync− neurons (Figures 4D and 4E), which is reflected by significantly positive regression slope values when firing rate and depolarization were plotted against ICI for all nSync− neurons tested (Figures 5C–5G). This is the first time that such subthreshold responses underlying the nSync− responses have been observed.

We performed correlation analysis of regression slope values between firing rate and MP for individual nSync+ and nSync− neurons, as shown in Figure 5G. A weak correlation was found for both nSync+ neurons ($r = 0.06$, $p = 0.86$) and nSync− neurons ($r = 0.36$, $p = 0.22$). In addition, we compared the basic neuronal properties of nSync+ and nSync− neurons (Table S1). The resting MP and spontaneous firing rate of nSync+ neurons were significant higher than those of nSync− neurons ($p < 0.05$). The first spike latency of nSync− neurons was shorter than that of nSync+ neurons ($p < 0.05$). There was no significant difference between these two populations in spike threshold ($p = 0.64$). When thresholds of the MP and firing rate were compared (Figure S3I), most nSync+ neurons were clustered near low-stimulus repetition frequencies, whereas most nSync− neurons were clustered near high-stimulus repetition frequencies. These

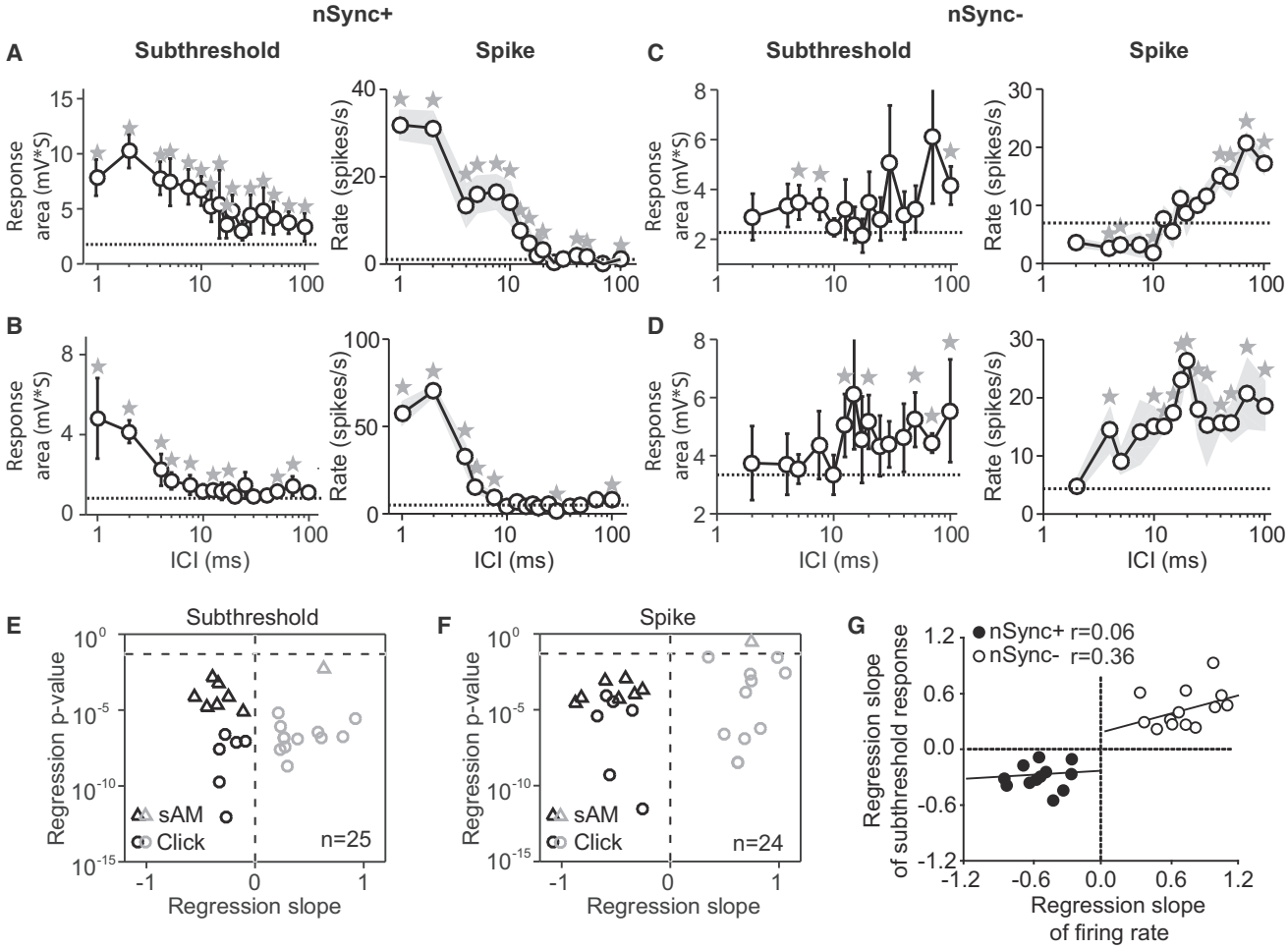

Figure 5. Classification of nSync+ and nSync– Neuronal Populations

(A–D) Subthreshold response magnitude (left) and firing rate (right) averaged over the duration of the click train and across trials plotted against the log scale of ICIs, for the four example neurons in Figures 4A–4D, respectively. Error bars and gray area show SDs. Dashed horizontal lines represent the mean spontaneous subthreshold responses (left) and the mean spontaneous firing rate (right) of each neuron. Asterisks indicate evoked responses that are significantly different from spontaneous responses. x axis label of (B) and (D) applies to (A) and (C).

(E and F) p value versus slope of linear regression fit of depolarization (E) and firing rate (F) on the log scale of ICIs (circle) and FMs (triangle) for all nSync+ (n = 13, black) and nSync− (n = 12, gray) populations (note one neuron only has subthreshold response). The horizontal dashed line indicates p = 0.05. Sync, Mixed, and other neuron types such as band-pass neurons were excluded in this analysis.

(G) Correlation of the regression slope between the mean firing rate and the mean subthreshold responses (as shown in E and F) for all nSync+ and nSync− neurons. nSync+ neurons, r = 0.06; nSync− neurons, r = 0.36. See also Figure S3I.

analyses further showed that nSync+ and nSync− neurons have distinct properties.

Non-synchronized Neurons Received Synchronized Inputs at Long, but Not Short, ICIs

There are two competing hypotheses proposed for the input synchronization underlying nSync+ responses that show increased firing with increasing stimulus repetition frequency. One hypothesis is that such neurons receive predominantly synchronized excitatory and inhibitory inputs at high repetition frequency or short ICIs such that the MP exhibits periodic fluctuations, which may facilitate the neuronal discharge at high repetition frequency (Gao and Wehr, 2015). An alternative hypothesis is that a large number of uncorrelated excitatory and inhibitory inputs are received by the nSync+ neuron at high repetition frequency or short ICIs, which elevates the MP to hover near the spiking threshold, thus generating non-synchronized sustained firing (Tan et al., 2014). To evaluate these two hypotheses, we closely examined the period histograms of both spike and subthreshold responses for nSync+ and nSync− neurons.

For the nSync+ neurons, we did not observe significant periodic fluctuations at short ICIs (Figures 6A and S4A), in contrast to a recent study on similar responses conducted in awake rats (Gao and Wehr, 2015). Instead, we observed periodic MP fluctuations only at long ICIs, as highlighted by the red dashed box (Figures 6A and S4A). For the nSync− neurons, we also

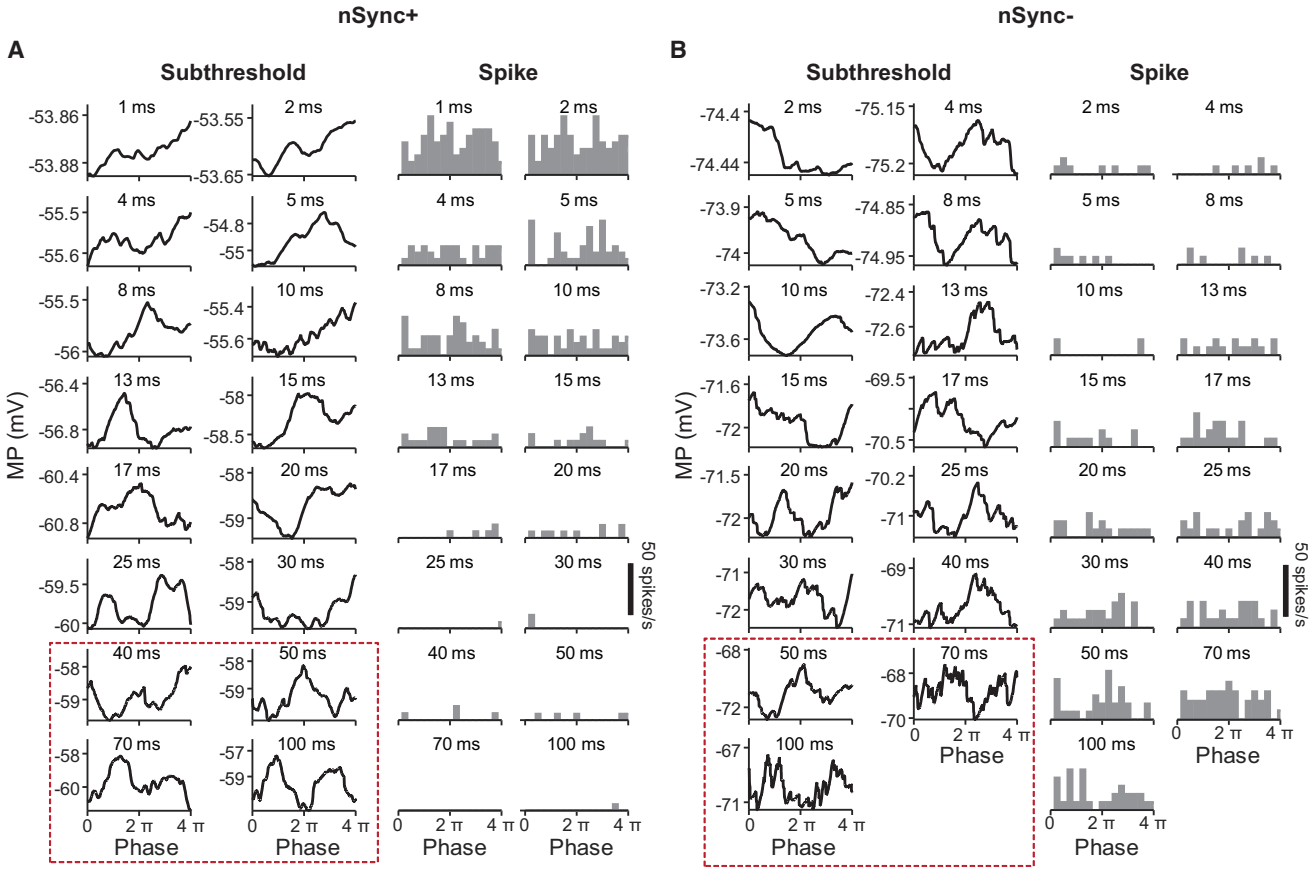

Figure 6. Cycle-Averaged Histograms of Subthreshold and Spiking Responses for nSync+ and nSync– Neurons

Cycle-averaged histograms of subthreshold (left, black) and spiking (right, gray) responses for two example neurons among four of those shown in Figure 4, a Sync+ neuron (A) and a Sync− neuron (B). Two complete cycles (0–4 π) are shown. A median filter was used to remove spikes to obtain the subthreshold response. Red dashed boxes highlight the synchronized subthreshold events. Scale bar in cycle-averaged histograms of spiking response (right panel) applies to all panels. See also Figures S3E–S3H, S4, and S6.

did not observe any periodic MP fluctuations at short ICIs; instead, this was found at long ICIs (Figures 6B and S4B). Weak MP fluctuations superposed on slightly sustained depolarization generated non-synchronized instead of synchronized spiking activities at long ICIs in nSync− neurons (Figures 4D–4F). We quantified the VS of MP and spiking activity for nSync+ and nSync− neuron populations. The VS of MP decreased with increasing stimulus repetition frequency (reciprocal of ICI) for both nSync+ ($r = -0.72$, $p < 0.001$) and nSync− ($r = -0.76$, $p < 0.001$) neurons (Figures S3E and S3F), but spiking activity did not show this trend (nSync+ neurons, $r = 0.17$, $p = 0.04$; nSync− neurons, $r = -0.20$, $p = 0.09$; Figures S3G and S3H). These results are consistent with the individual examples shown in Figures 6 and S4.

Considering that different spike removal methods in the analysis may affect the period histograms of subthreshold response at short ICIs, we tested both linear interpolation (Zanos et al., 2011) and median filter (Jagadeesh et al., 1997; Priebe et al., 2004) methods to remove spikes from intracellular recordings (see Experimental Procedures). We did not observe periodic fluctuations of the MP at short ICIs for either method (Figure S5).

We also performed Fourier analysis on the individual trials across ICIs without removing spikes where we observed significant peaks at the low instead of high repetition frequencies (Figure S6) for both nSync+ and nSync− neurons. These results indicated that neurons with non-synchronized responses received synchronized inputs at low, but not high, repetition frequency of time-varying stimuli via presumably thalamocortical and/or intracortical inputs.

Magnitude of the MP Determines Firing Patterns of nSync+ and nSync– Responses

Our intracellular recording results showed distinct subthreshold mechanisms underlying nSync+ and nSync− responses: nSync+ neurons exhibited sustained depolarization at short ICIs, whereas nSync− neurons displayed hyperpolarization at short ICIs and sustained depolarization at long ICIs (Figure 4). To compare the MP dynamics between nSync+ and nSync− neurons, we plotted the period histograms of the MP (cycle-averaged subthreshold responses) across ICIs on the same voltage scale for four representative non-synchronized neurons (Figure 7). In the range of short ICIs (<20 ms), the MP of the nSync+ neurons

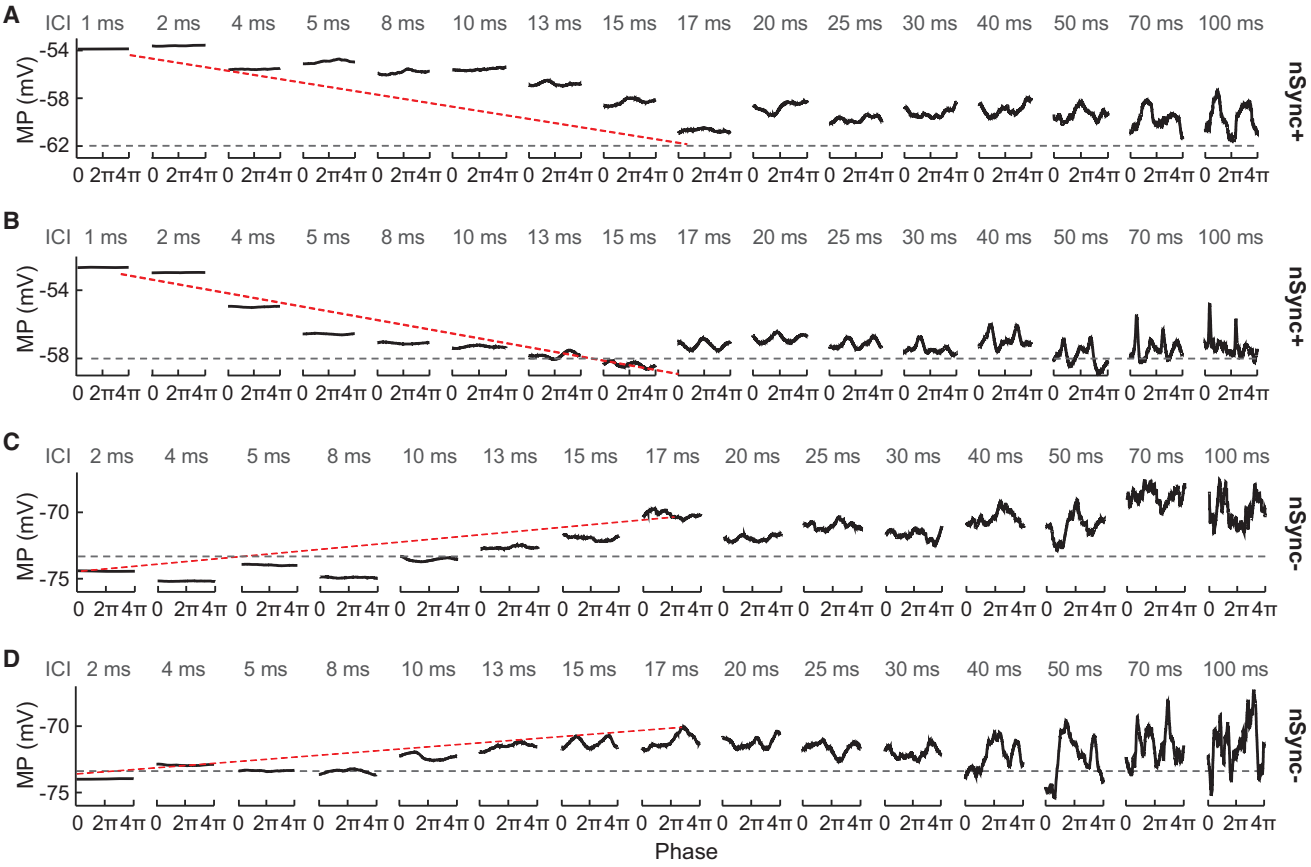

Figure 7. Positive/Negative Monotonically Varying MP at Short ICIs for nSync+ and nSync– Neurons

Cycle-averaged histograms of the subthreshold responses for the four example neurons shown in Figure 4 (nSync+, A and B; nSync−, C and D). A median filter was used to remove spikes to obtain the subthreshold response. The y axis scale is identical for each neuron. Two complete stimulus cycles (0–4 π) are shown. The gray dashed line indicates the resting MP of each individual neuron. The red dashed line indicates the trend of MP change across short ICIs (<20 ms). See also Figures S3J and S7.

increased monotonically with decreasing ICI (Figures 7A and 7B), whereas the MP of the nSync− neurons decreased with decreasing ICIs (Figures 7C and 7D). We calculated the MP slope changes in period histograms across short ICIs (<20 ms) for nSync+ and nSync− neurons. The slope values were negative for nSync+ neurons (−0.15 ± 0.07, $p < 0.001$) while positive for nSync− neurons (0.11 ± 0.07, $p < 0.01$) (Figure S3J). These trends in the MP corresponded to increased spiking activity in nSync+ neurons and suppressed spiking activity in nSync− neurons with decreasing ICI at short ICIs (Figure 4). Correlation analyses between firing rate and MP showed that, as expected from the known signal transmission property of a neuron, the MP of both nSync+ and nSync− neurons was transformed to firing rate by a power law, such that the firing rate was proportional to the voltage above resting MP (Figure S7). These observations indicate that the MP of nSync+ and nSync− neurons at short ICIs determines their firing patterns that vary with ICIs. Moreover, the period histograms of the MP for both nSync+ and nSync− neurons exhibited large fluctuations at long ICIs (>20 ms), in contrast to subtle fluctuations at short ICIs (Figure 7), suggesting that they received more synchronized inputs at long than short ICIs.

Simulating Synchronized and Non-synchronized Responses in A1

The present study provided a rich set of intracellular recordings of responses to click trains in auditory cortex neurons. In order to provide a comprehensive mechanistic explanation of our intracellular recording results, we used a leaky integrate-and-fire model of A1 neurons to simulate the neuronal response types observed in this present study (Figure S8). This model shared some parameters with the model used in the Bendor (2015) study, but also included new parameters and manipulations that were crucial to simulate the complete range of firing patterns and MP dynamics that were observed in the present study. Computational models used in previous studies simulated Sync and nSync+ responses based on extracellular recordings from A1 of awake marmosets (Bendor, 2015) or intracellular recordings from A1 of awake rats (Gao and Wehr, 2015). However, these models did not simulate or predict the two opponent rate-coding neuronal populations (nSync+ and nSync−) that we have observed in A1 of awake marmosets both extracellularly and intracellularly. We identified four key parameters in our model (out of 18 parameters) that were

critical to producing outcomes that matched the intracellular recording data from awake marmosets: (1) I/E delay, which was the temporal delay of inhibitory and excitatory inputs; (2) I/E ratio, which was the ratio between the magnitude of inhibitory and excitatory inputs; (3) synaptic time constant, which was the rising time of synaptic inputs; and (4) saturation time of excitation, which provided a ceiling on the excitatory current into the neuron. These four parameters were varied in our simulation. The synaptic time constant and the saturation time of excitation were crucial for generating the nSync− responses, which were not modeled in any previous studies (e.g., Bendor, 2015). Both of these parameters represent plausible scenarios for neural mechanisms underlying cortical responses to time-varying stimuli. The synaptic time constant represents major types of receptors, including AMPA- and $GABA_A$-based short time constant and NMDA-based long time constant (Kleppe and Robinson, 1999). The saturation time of excitation models the adaptation of synaptic inputs, for example, depletion of vesicles at the synapse or adaptation at lower parts of the pathway. Since the ratio of the excitatory and inhibitory saturation times is more important, we fixed the saturation time of inhibition to an intermediate value and varied the excitatory saturation time.

With this model and above-mentioned parameter manipulations, we were able to simulate the firing patterns of Sync, Mixed, nSync+, and nSync− responses to click trains with varying ICI (Figures 8A–8D), as well as corresponding MP dynamics. The simulated MP dynamics, such as periodic depolarization of Sync and Mixed neurons, sustained depolarization of nSync+ neurons, and hyperpolarization of nSync− neurons, were consistent with our intracellular recording results (Figures 2 and 4). We categorized the simulated responses into four types by the slope of the linear regression of firing rate on the log scale of ICIs and Rayleigh statistics of firing rate (Figure 8E; see Experimental Procedures). We then systematically varied the four key parameters of the model to study how each response type was created. We found that Sync, Mixed, nSync+, and nSync− responses occupied four distinct regions on the model's parameter space (Figures 8F and S9). Specifically, synaptic inputs with short time constant ($\leq$15 ms) captured Sync, Mixed, and nSync+ responses (upper portion of Figure 8F). The nSync+ response had a short saturation time of excitation (upper left corner of Figure 8F), Sync response had a long saturation time of excitation (upper right corner of Figure 8F), and Mixed response was located in between. However, the nSync− response was generated when the synaptic inputs had a long time constant ($\geq$15ms) and a long saturation time ($\geq$14 ms) (lower right corner of Figure 8F). By increasing the I/E ratio (Figure 8F, yellow arrows), nSync+ responses tended to become the other three types and Mixed responses tended to become Sync responses. By increasing the I/E delay (Figure 8F, blue arrow), nSync− responses tended to become Sync responses. In summary, this computational model could reproduce all four neuronal types in response to time-varying stimuli with biologically meaningful parameters and minimum assumptions, which has direct implications for the cellular mechanisms underlying these responses in auditory cortex.

DISCUSSION

We developed a novel intracellular recording technique in this study to investigate the cellular mechanisms underlying temporal coding schemes for time-varying stimuli in A1 of awake marmosets. By using this technique, we observed distinct subthreshold responses underlying synchronized and two types of non-synchronized responses. A major conceptual advance of our study is that it provides a cellular explanation of the opponent rate-coding model, which has been demonstrated in both auditory and somatosensory cortices with extracellular recording. Specifically, we suggested that the responses of nSync+ neurons (monotonically increasing firing rate with increasing stimulus repetition frequency) were due to sustained depolarization at high repetition frequency as a result of temporal integration with short integration windows, whereas the responses of nSync− neurons (showing the opposite trend) were formed by hyperpolarization at high repetition frequency but sustained depolarization at low repetition frequency as a result of temporal integration with long integration windows. The combination of excitatory and inhibitory inputs at different timescales allows the auditory cortex to represent time-varying signals through these two opponent neuronal populations. We were also able to simulate both firing patterns and MP dynamics of the four neuronal response types, as observed in our intracellular recording experiments using a computational model of A1 neurons; in particular, the nSync− response has never been studied intracellularly and computationally. Our results provide new insights into the cellular mechanisms underlying temporal coding strategies in the primate auditory cortex.

Intracellular Recording from Awake Marmosets

Nonhuman primates are valuable animal models for studying neural mechanisms for perception, cognition, and social communication. However, low success rate and poor recording stability have hampered the application of intracellular recording techniques in studies of awake nonhuman primates. The co-axial intracellular recording technique that we developed overcame these limitations and allowed us to stably and reliably record from the cortex of awake marmosets with minimal damage to the brain (without dura removal) over many sessions. With this technique, we were able to record intracellularly dozens of neurons in each marmoset under the awake condition as opposed to only obtaining a few units per animal in a typical rodent study. This technique allows us to simultaneously record the MP dynamics and firing patterns of individual cortical neurons across different brain areas and cortical layers in order to study the relationship between synaptic inputs and spiking output of individual neurons in awake marmosets. The direct observations of hyperpolarized MP (Figures 4D–4F) and recordings from fast-spiking interneurons (classified by spike waveforms; see Table S2) provide valuable information on contributions by inhibitory inputs to cortical neurons. This breakthrough in recording technique made it possible to systematically study the cellular mechanisms underlying temporal coding schemes. The development of this method took advantage of our laboratory's decade-long experience in performing single-neuron chronic recordings in awake marmosets (Lu et al., 2001a; Wang et al., 2005). This

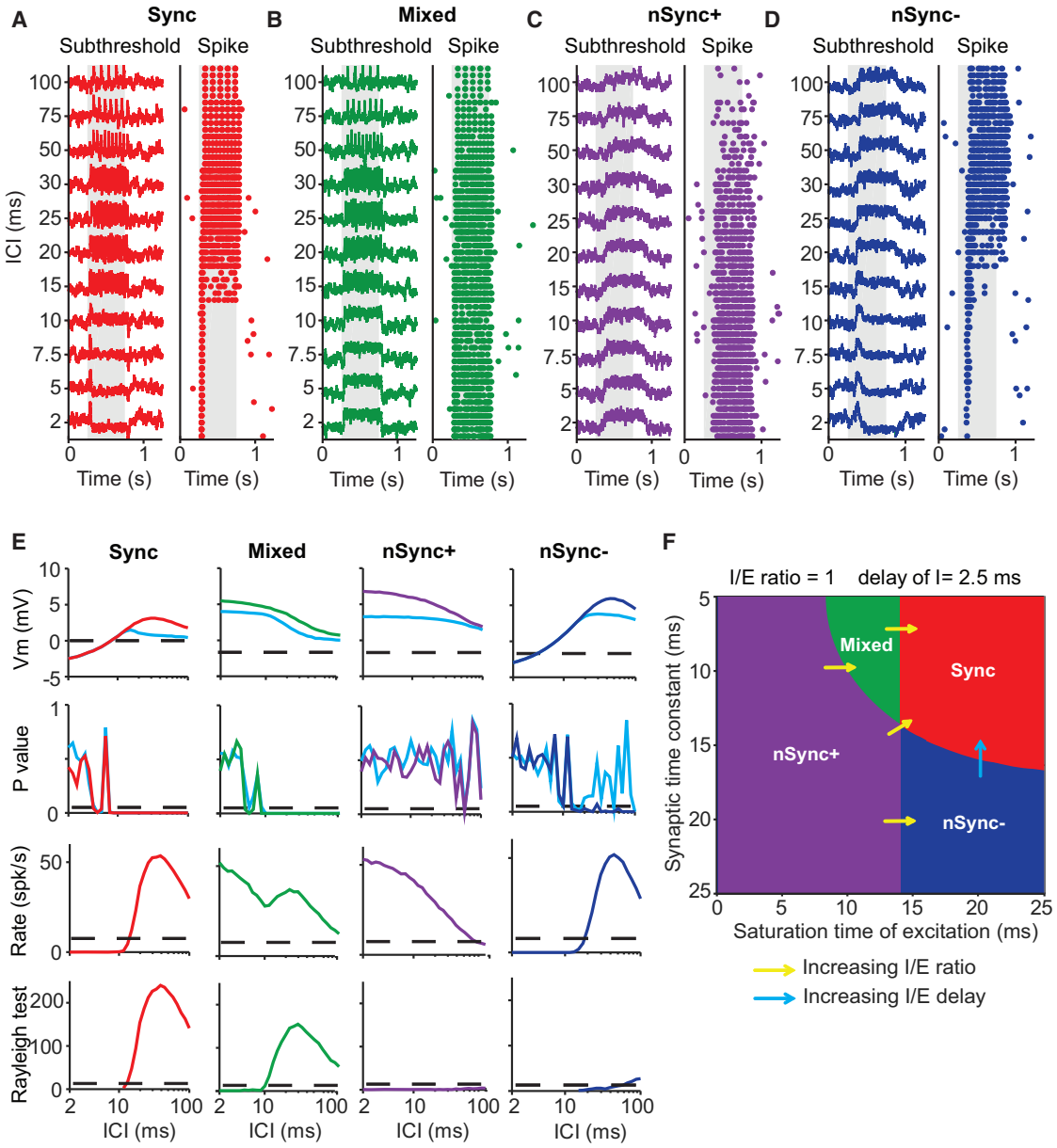

Figure 8. Computational Simulation of A1 Response to Repetitive Stimuli

(A–D) Examples of simulated Sync (A, red), Mixed (B, green), nSync+ (C, purple), and nSync− (D, blue) responses to click train with varying ICI. For each example, simulated mean subthreshold responses of five repetitions at each ICI (left) and raster plots of simulated discharge (right) are shown. Stimulus duration is indicated by the gray shaded area.

(E) Four indices were used to quantify simulated neuronal responses as a function of ICI: (1) subthreshold response amplitude (first row), (2) significance test of the MP periodicity (second row), (3) firing rate (third row), and (4) Rayleigh statistics (fourth row). Dashed horizontal lines indicate the magnitude of spontaneous MP fluctuations (first row), significant p value (0.05, second row), spontaneous firing rate (third row), and significant Rayleigh test value (13.8, fourth row). In the first and second row, blue indicates that the MP was measured with spikes generated simultaneously. Other colors indicate that the MP was measured with spikes disabled.

(F) Neuronal types differentiated by the model's four key parameters. A 2D cross-section of this 4D parameter space was shown (with fixed I/E ratio = 1 and delay of I = 2.5 ms). Arrows indicate, qualitatively, how the type would change when the other two parameters were varied. See also Figures S8 and S9.

unique approach to conducting intracellular recording under the awake state can be adapted to study other brain regions in marmosets or in the brains of similar sized animals. However, sharp electrode intracellular recording is limited in parsing excitatory inputs from inhibitory inputs. Although the MP of a recorded neuron can be manipulated by injecting a DC current to change the strength of excitation and inhibition, it remains challenging to perform such manipulations in awake animals.

Non-synchronized Responses and Temporal-to-Rate Transformation in Auditory Cortex

A distinct property of neurons in the auditory cortex of awake animals is sustained firing in response to specific acoustic stimulation (Mickey and Middlebrooks, 2003; Wang et al., 2005). However, the cellular mechanisms underlying such responses have remained largely elusive because of the difficulties in measuring subthreshold activity in awake animals. Synchronized responses evoked by repetitive stimuli were observed in auditory cortex under both anesthetized and awake states (Joris et al., 2004). In contrast, non-synchronized responses to repetitive stimuli have only been observed in A1 under awake conditions in several species such as marmosets (Bendor and Wang, 2007; Lu et al., 2001b), cats (Dong et al., 2011), and rats (Gao and Wehr, 2015). Unlike the synchronized responses, the non-synchronized responses represent processed instead of preserved temporal information, suggesting that cortical processing of sound streams operates on a "segment-by-segment" basis rather than on a "moment-by-moment" basis, as found in the auditory periphery (Wang et al., 2008). We argued previously that the transformation from temporal to rate code is necessary for complex cortical integration since higher-level processing tasks require temporal integration over specific time intervals (Wang, 2007).

Observations from extracellular recordings suggested that neurons in A1 of awake animals use a combination of monotonically increasing or decreasing non-synchronized discharges (nSync+ and nSync−) to encode acoustic flutters (~10–45 Hz) (Bendor and Wang, 2007). In the present study, we found distinct cellular mechanisms underlying the formation of nSync+ and nSync− responses, suggesting that distinct synaptic inputs and neural circuits may be involved in creating these responses. The discovery of these two types of non-synchronized responses is significant because it allows an opponent model of rate coding by two populations of neurons whose firing rates change in opposite directions as stimulus repetition frequency increases. This overcomes a crucial limitation of firing rate-based representations because the firing rate of an auditory neuron depends on other parameters such as sound level. Moreover, we found the subthreshold response was able to entrain to faster temporal repetition frequencies than spiking activity, which provided direct evidence to support the temporal-to-rate transformation from MGB to A1, as suggested in our previous studies (Bartlett and Wang, 2007; Lu et al., 2001b; Wang, 2007). The findings here may apply to sensory coding mechanisms in vision and touch since both sensory modalities require the temporal-to-rate transformations to represent stimuli characteristics (spatial frequency, vibration, texture).

We have previously suggested that the slowdown in synchronization in auditory cortex is necessary for multi-sensory integration as auditory information is encoded subcortically at much higher temporal modulation rates than the rates at which visual or tactile information is encoded at the periphery, but the limit of firing synchronization is similar across primary sensory cortical areas (Wang et al., 2008). This notion could apply to the synchronized neurons that are found in A1, somatosensory (S1), and visual (V1) cortices. It is less clear what role non-synchronized neurons play in multi-sensory integration between auditory and visual systems because there is little evidence of non-synchronized neurons in V1 (Montemurro et al., 2008). Non-synchronized neurons may be involved in multi-sensory integration between auditory and somatosensory systems because of their shared properties.

Comparison with Previous Studies

Until recently, neural responses to time-varying signals in auditory cortex were studied mostly in anesthetized animals. Under anesthesia, auditory cortex responses are dominated by synchronized firing patterns (Joris et al., 2004). Under unanesthetized conditions, a diverse range of firing patterns has been observed in auditory cortex (Wang et al., 2008). Using single-unit extracellular recording, Lu et al. (2001b) reported non-synchronized firing in A1 of awake marmosets in response to click train stimuli at high repetition frequency (referred to as nSync+ response in the present study). Several years later, Bendor and Wang (2007) also used single-unit extracellular recording in awake marmosets and discovered that there were two types of non-synchronized responses in the core region of auditory cortex and named them "positive-monotonic" and "negative-monotonic" non-synchronized firing, respectively, after the convention introduced by Romo and colleagues in the somatosensory cortex where similar non-synchronized firing patterns had been observed (Bendor and Wang, 2007; Romo and Salinas, 2003). We adapted the terminology of "positive-monotonic" and "negative-monotonic" responses in the present study and referred to them as nSync+ and nSync−, respectively. The positive-monotonic response is similar to non-synchronized firing observed in Lu et al. (2001b), whereas the negative-monotonic response shows the opposite trend as the positive-monotonic response in that it increases firing rate as stimulus repetition frequency decreases. The observation of the negative-monotonic response in auditory cortex was one of the more surprising findings in this line of literature, as this type of response is not readily expected or explained by temporal integration models. The nSync− response has so far only been observed in awake marmoset auditory cortex in Bendor and Wang (2007) and the present study. Bendor and Wang (2007) also showed that A1 contains more synchronized neurons, whereas the rostral areas contain more non-synchronized neurons, which suggested that there is a further temporal-to-rate coding transformation along the caudal-to-rostral axis of the primate auditory cortex. The differences in the proportions of synchronized and non-synchronized neurons in A1 as reported in the present study and previous studies (Lu et al., 2001b, Bendor and Wang, 2007) are likely due to the acoustic stimuli used (see Experimental Procedures).

Recently, Gao and Wehr (2015) conducted a study in awake rats using a similar stimulus protocol as used in Lu et al. (2001b) and observed non-synchronized firing in A1 similar to nSync+ response reported in Lu et al. (2001b) and the present study. However, nSync− responses were not observed in the Gao and Wehr (2015) study. The reason for the lack of nSync− responses in rodents is unclear. It could be due to the relatively small sample size from each animal or that such responses are specific to the primate auditory cortex. However, it has remained unclear how A1 neurons in marmosets are able to respond to time-varying stimuli with these two different types

of non-synchronized neurons, especially the negative-monotonic response. Our work combined high-quality intracellular recordings with a computational model to delineate the neuronal coding mechanisms underlying the diverse temporal coding schemes to time-varying stimuli in A1 of awake marmosets.

We found sustained depolarization underlying sustained and non-synchronized firing in A1 of awake marmosets, which is consistent with a previous in vivo study in awake rats (Gao and Wehr, 2015) and an in vitro study in ferrets (McCormick et al., 2003). The intracellular recording study by Gao and Wehr (2015) not only confirmed the earlier observation of non-synchronized firing in awake marmosets by Lu et al. (2001b) but also provided possible explanations of mechanisms by which A1 neurons might perform temporal-to-rate transformation. This question was also investigated in the present study in awake marmoset A1. Gao and Wehr (2015) reported periodic MP fluctuations at high repetition frequency (up to 500 Hz or 2 ms ICI) from neurons exhibiting nSync+ responses. Contrary to their finding, we observed no periodic MP fluctuations at such high repetition frequency for both nSync+ and nSync− neurons (Figures 6 and S4). It is important to clarify the potential differences of methodology in analyzing the periodicity of the MP. In the Gao and Wehr (2015) study, the periodic histogram of the MP was calculated without spike removal. As the non-synchronized firings may reduce the periodicity of the MP by averaging the MP cross trials and cycles, we calculated the periodic histogram of subthreshold response after the spikes were removed by applying both median filter (Jagadeesh et al., 1997; Priebe et al., 2004) and linear interpolation (Zanos et al., 2011) methods, respectively. We did not observe periodic MP fluctuations at short ICIs for nSync+ and nSync− responses by either spike removal method listed above (Figure S5). To avoid affecting the spectral content of the data through spike removal at short ICIs, we also applied fast Fourier transform (FFT) on the raw data without removing spikes to examine whether periodic events existed at shorts ICIs. Through this method, we found that periodicity in the MP was evident at long ICIs, but not observed at short ICIs (Figure S6). These observations were consistent with the suggestion that thalamocortical projections provide synchronized inputs at long ICIs, but not at short ICIs, based on previous extracellular recording studies (Bartlett and Wang, 2007; Wang et al., 2008). However, the periodic MP at long ICIs in non-synchronized neurons did not result in synchronized firing (Figure 6) because in some neurons, the resting MP was far below the spike threshold such that synaptic inputs (periodic or not) failed to reach the spike threshold (e.g., Figures 4A and 4B). In other neurons, periodic inputs were too weak or inconsistent to cause periodic spiking activity (Figures 4D and 4E). Thus, firing synchrony was diminished in both of these scenarios.

In a modeling study by Bendor (2015), an integrate-and-fire neuron model was used to investigate the role of inhibition-forming temporal and rate representations in A1 based on the extracellular recording data from awake marmosets. The model showed that strong inhibition-lagging excitation produced synchronized responses, and weak net excitation due to concurrent and balanced excitation-inhibition interplay produced non-synchronized responses (comparable to nSync+ in the present study). No attempt was made to model the subthreshold events, as no such data were available until the present study. Rabang and Bartlett (2011) demonstrated an alternative model for generating temporal and rate representations in auditory thalamus: large inputs with synaptic depression created synchronized responses while weak inputs with plasticity (synaptic depression of AMPA receptors and synaptic facilitation of NMDA receptors) generated mixed and non-synchronized responses (comparable to nSync+ in the present study) (Rabang and Bartlett, 2011). Gao and Wehr (2015) also used a model to demonstrate how periodic MP fluctuations on the sustained depolarization could generate sustained firing, but it did not explain the MP dynamics of non-synchronized response across ICIs. Importantly, none of the above computational models simulated or predicted the firing pattern of nSync− neurons and corresponding subthreshold events.

To elucidate potential biophysical parameters that give rise to the diversity of neuronal responses observed in these experiments, we used a neuronal model with realistic biophysical parameters to simulate both the MP dynamics and firing patterns of the four types of neuronal responses by varying a minimum number of the most crucial parameters. Considering synaptic adaptation and depression as well as NMDA receptors, which also played important roles in synaptic transmission besides AMPA and $GABA_A$ receptors, we extended the model use in the Bendor (2015) study by adding two additional parameters: a variable synaptic time constant and saturation time of excitatory inputs (see Experimental Procedures). By adding these parameters, we were able to capture both the MP dynamics and firing patterns of the complete diversity of responses to stimulus repetitions observed in A1 of awake marmosets including Sync, Mixed, nSync+, and nSync− responses across ICIs. By allowing longer time constant and inhibition to saturate at a shorter ICI than excitation, we were able to produce both spiking and subthreshold responses of the nSync− neuron, which was one of the most novel experimental findings on temporal-to-rate transformations in A1 and has not been simulated or predicted by any previous modeling work. Our modeling suggested that the diverse responses observed in our experiments were controlled by a particular set of biophysical parameters of A1 neurons, which provides insights beyond the experimental data presented. These results may help future experiments using different techniques to validate these parameters and discover additional parameters that may play important roles in generating A1 responses. We recognize that our model does not rule out other nonlinear neuronal properties that could potentially contribute to the generation of synchronized and non-synchronized responses in auditory cortex. Furthermore, sharp electrode recording has limitations in isolating excitatory inputs from inhibitory inputs. Future studies using techniques such as voltage-clamp recording may provide additional experimental data to constrain and improve the models of firing patterns in auditory cortex.

EXPERIMENTAL PROCEDURES

All experimental procedures were approved by the Johns Hopkins University Animal Use and Care Committee.

Intracellular Recording Procedures

Experiments were conducted in awake marmosets using the chronic preparation previously developed in our laboratory (Lu et al., 2001a; Wang et al., 2005) (see Supplemental Information for details on animal preparation). Intracellular recordings were made in the superficial layers (300–1,200 μm) of A1 through the intact dura using a concentric sharp electrode and guide tube assembly (Figure 1A). The recording pipette was made of quartz glass (inner diameter [ID] = 0.5 mm, outer diameter [OD] = 1.0 mm, Sutter Instrument) rather than the traditional borosilicate glass to improve the strength of recording electrodes in order to penetrate through the intact dura without its removal (Figure 1B). This allowed us to record over five to seven sessions in a single craniotomy with minimal damage to the cortex. The recording pipette was pulled by a laser puller (P-2000, Sutter Instrument) to a resistance of 90–120 MΩ and back-filled with 3.0 M KAc (pH 7.6, Sigma). We used a co-axial guide tube made of borosilicate glass pipette (ID = 1.1 mm, OD = 1.5 mm, Sutter Instrument) concentric to the recording electrode to provide protection for the sharp electrode tip, both of which were attached to a custom-made holder (Figure 1A). The electrode assembly was advanced perpendicularly relative to the brain surface with a motorized manipulator (DMA1510, Narishige). Once the desired recording depth was reached (300∼400 μm below the dura), the recording electrode was manually decoupled from the guide tube, which was temporarily fixed to the recording chamber with dental impression material (Kerr). At this point, the recording electrode can move independently of the guide tube and was advanced into the cortex. The recording electrode was lowered at 4 μm steps paired with short buzzes (50 ms) of electric current injection into the electrode to aid penetration. An abrupt drop in voltage signaled penetration of the cell membrane. After the micropipette was stabilized for a few minutes inside the cell and the voltage stayed below –50 mV, we commenced to present auditory stimuli while recording both the spikes and the MP dynamics, as shown in Figure 1C. The electrical signals were amplified using Axoclamp 2B (Molecular Devices), digitized (RX6, Tucker-Davis Technologies), analyzed, and saved using custom programs written in MATLAB (Mathworks). Each daily recording session lasted 4–5 hr. All recording sessions were conducted within a double-walled soundproof chamber (Industrial Acoustics). The interior of the chamber was covered by 3 in acoustic absorption foam (Sonex).

Acoustic Stimuli

Acoustic signals were generated digitally in MATLAB (MathWorks) at a sampling rate of 97.7 kHz with custom software, converted to analog signals (Tucker-Davies Technologies), power amplified (Crown Audio), attenuated (Tucker-Davies Technologies), and delivered in free-field through a speaker (B&W-600S3) located approximately 1 m in front of the animal. Once a neuron was held, its basic tuning properties, such as best frequency (BF) and best level (BL), were determined. Pure tones 100 ms in duration with 5 ms cosine ramps were presented spanning 3–4 octaves around a manually determined center frequency in 0.1-octave or smaller steps. The range of the sound level was from −10 to 80 dB SPL in 10 dB steps. The BF of a neuron was defined as the centroid of the frequency tuning curve at 40 dB SPL. Many A1 neurons in awake marmosets show non-monotonic rate-level functions (Sadagopan and Wang, 2008). The BL of a neuron was defined as the sound level that elicited the maximal firing rate at BF. After the BF and BL of a neuron were determined, two types of temporally modulated sounds were played in randomized blocks for three to five repetitions. The first type was sAM tone. The carrier frequency, set at a neuron's BF, was held constant while its amplitude was modulated by a sinusoid signal. The MF varied between 2 and 512 Hz on a logarithmic scale. Another type of stimulus was narrow-band click train (Gaussian clicks), which had a sinusoid carrier at a neuron's BF that was amplitude modulated by a Gaussian envelope, with constant ICI ranging from 2 to 100 ms (repetition frequency between 10 and 500 Hz). The bandwidths of the Gaussian clicks were controlled by the SD parameter, σ, and ranged from 0.1 to 0.3. A larger σ value gave a wider temporal envelope and a narrower spectral peak. The duration of sAM and Gaussian click train was 500 or 1,000 ms, although it was sometimes longer.

The range of modulation or repetition frequency used in the present study was similar to that used in an earlier study (Lu et al., 2001b) that first reported synchronized and non-synchronized responses in awake marmoset A1, but higher than that used by Bendor and Wang (2007) (up to 48 Hz). Because non-synchronized neurons were more easily identified by the time-varying stimuli with higher repetition or MF, these differences in stimulus repetition frequency explain different proportions of synchronized and non-synchronized neurons reported among above-mentioned studies. The present study reported 52 intracellularly recorded A1 neurons, including 18 synchronized, 25 non-synchronized, and 9 Mixed neurons (35%, 48%, and 17%, respectively). Lu et al. (2001b) reported 94 extracellularly recorded A1 neurons, including 36 synchronized, 50 non-synchronized, and 8 Mixed neurons (38%, 53%, and 9%, respectively) (see Lu et al., 2001b; Figure 3). Bendor and Wang (2007) reported 111 extracellularly recorded A1 neurons, including 64 synchronized, 36 non-synchronized, and 11 Mixed neurons (58%, 32%, and 10%, respectively) (see Bendor and Wang 2007; Table S1).

Data Analysis

Neuronal signals were continuously digitized and saved onto a computer during each stimulus presentation, including pre-stimulus and post-stimulus windows. Both MP and spike data were analyzed offline using custom software implemented in MATLAB (Mathworks). Spikes were detected online by setting a threshold of at least 30 mV above the baseline of the MP. The spiking activities analysis methods used were the same as in our previous publications (Lu et al., 2001a; Bendor and Wang, 2008; Sadagopan and Wang, 2008). In brief, average discharge rates were calculated over the entire stimulus duration and the mean spontaneous rate (estimated over the entire stimulus set) was subtracted in all analyses. The criterion for a significant stimulus-driven spiking response was defined as an averaged discharge rate two SDs above the mean spontaneous discharge rate. To obtain the subthreshold response, action potentials were removed from the intracellular recording signal by using two methods, respectively: (1) 4-ms median filter (Jagadeesh et al., 1997; Priebe et al., 2004), in which each digitized point of intracellular recording signal was replaced with the median of itself and the 20 values surrounding it, consequently removing action potentials and leaving the smaller and slower fluctuations in MP largely unchanged; and (2) linear interpolation (Zanos et al., 2011), in which action potentials were first detected and the signal in 3 ms windows centered at the peak of action potentials was deleted, and then a linear interpolation was performed to fill the gap. Figure S5 shows examples of these analyses. The baseline of the MP was defined by the mean value of MP in an analysis window of 50 ms with minimal fluctuations by sliding the analysis window at every 10 ms step throughout the pre-stimulus duration. The magnitude of subthreshold response was defined by the area of depolarization or hyperpolarization over the stimulus duration. The spontaneous subthreshold response was defined by the mean area of MP fluctuations before sound presentation over the entire stimulus set. The criteria for a significant subthreshold response were defined as an averaged subthreshold area two SDs above the spontaneous subthreshold response.

The VS was calculated to quantify synchronized responses for both spikes and subthreshold responses. Onset responses (0–100 ms) were excluded from the calculation of VS. The statistical significance of synchronized spiking activity was determined by Rayleigh statistic (>13.8, $p < 0.001$) (Lu et al., 2001b; Mardia and Jupp, 2000). For each neuron with synchronized or mixed response to sAM or Gaussian click stimuli, a synchronization boundary was calculated from the Rayleigh statistic versus MF or ICI curve and defined as the shortest ICI or highest MF above the Rayleigh threshold value of 13.8. The synchronization of the subthreshold response to a stimulus could not be directly assessed with a Rayleigh test due to the dependence on sample rate.

All values are expressed as mean ± SD unless otherwise specified. A one-way ANOVA, with Student's t test, was used for an analysis of the data. p values with $p < 0.001$, $p < 0.01$, or $p < 0.05$ were considered statistically significant in respective tests, as indicated where appropriate. We tested statistical significance of MP response (without spike deletion) at the click frequency f by comparing the energy at f with the background noise energy in the vicinity of f.

Computational Model

We developed a leaky integrate-and-fire model of a single cortical neuron, which was based on a model proposed by Bendor (Bendor, 2015) (see Supplemental Information for more details on the model). The model was tested with a periodic click train with varying ICI (1∼100 ms). Each click was modeled as a

change of excitatory and inhibitory conductance, which was computed by convolving the click train with a rise-fall synaptic response and accounting for saturation of the synapses. The system noise was modeled by injecting a random current into the neuron. We were able to reproduce the intended range of responses by fixing most parameters and varying only four degrees of freedom: (1) I/E delay, which was the temporal delay of inhibitory and excitatory inputs; (2) I/E ratio, which was the ratio between the magnitude of inhibitory and excitatory inputs; (3) synaptic time constant, which was the rising time of synaptic inputs varying from 5 to 25 ms; and (4) saturation (T_{sat}) time of excitatory inputs, which was modeled with a per-synapse vitality v_j parameter that is reset to zero when the stimulus S was 1 (indicating a click) and recovered exponentially:

$$\frac{d\,v_j}{dt} = \frac{1 - v_j}{\tau_{sat,\,j}} - S\,\delta\,v_j.$$

We set T_{sat} to 7.5 ms for inhibitory synapses and varied it between 0 and 25 ms for excitatory synapses. Among the above-mentioned four parameters, I/E delay and I/E ratio were used and varied by the Bendor (2015) model; the synaptic time constant was in the Bendor (2015) model but not varied; the saturation time of excitatory inputs was not used in the Bendor (2015) model. We also eliminated the global synaptic strength by adjusting it such that the maximum firing rate was about 50–55 spikes/s over all click trains ranging from 1 to 100 ms ICI. Other parameters were fixed to yield realistic examples of the four neuronal types. See the Supplemental Information for implementation details.

Neuronal Response Type Classification

Neuronal responses were classified into four types based on previous studies (Bendor and Wang, 2007; Lu et al., 2001b): Sync, Mixed, nSync+, and nSync− responses. A Rayleigh statistic above 13.8 for at least one ICI at or below 40 ms over a stimulus duration of 5 s (for simulated neurons) or averaged over several 0.5 s iterations (for intracellular recorded neurons) was required for Sync and Mixed neurons. These neurons were categorized as Sync if the maximum firing rate for ICIs at or below 5 ms was less than half the maximum firing rate, and as Mixed otherwise. Neurons were categorized as nSync+ if a linear regression of the firing rate on the log of click repetition rate yielded a positive slope on the range from 1 to100 ms ICI, and as nSync− if the regression had a negative slope.

SUPPLEMENTAL INFORMATION

Supplemental Information includes Supplemental Experimental Procedures, nine figures, and two tables and can be found with this article online at http://dx.doi.org/10.1016/j.neuron.2016.07.004.

AUTHOR CONTRIBUTIONS

L.G. and X.W. designed the research and developed the intracellular recording method in awake marmosets. L.G. collected the majority of the intracellular data; Y.W. collected part of the intracellular data; L.G. analyzed the data; K.K. performed the modeling work; and L.G., Y.W., and X.W. wrote the manuscript.

ACKNOWLEDGMENTS

We thank Xinjian Li at NIH for writing the MATLAB analysis programs and discussing and analyzing the data, and Seth Koehler and Michael Osmanski at Johns Hopkins University for comments on the manuscript. We also thank Shiyong Huang, Kaiwen He, and Alfredo Kirkwood at Johns Hopkins University for providing access and technical support for the laser-based pipette puller (Model P-2000). This work was supported by NIH grant DC03180 (X.W.).

Received: March 14, 2016
Revised: May 25, 2016
Accepted: June 28, 2016
Published: July 28, 2016

REFERENCES

Agamaite, J.A., Chang, C.-J., Osmanski, M.S., and Wang, X. (2015). A quantitative acoustic analysis of the vocal repertoire of the common marmoset (*Callithrix jacchus*). J. Acoust. Soc. Am. *138*, 2906–2928.

Aitkin, L.M., Merzenich, M.M., Irvine, D.R., Clarey, J.C., and Nelson, J.E. (1986). Frequency representation in auditory cortex of the common marmoset (Callithrix jacchus jacchus). J. Comp. Neurol. *252*, 175–185.

Bartlett, E.L., and Wang, X. (2007). Neural representations of temporally modulated signals in the auditory thalamus of awake primates. J. Neurophysiol. *97*, 1005–1017.

Bendor, D. (2015). The role of inhibition in a computational model of an auditory cortical neuron during the encoding of temporal information. PLoS Comput. Biol. *11*, e1004197.

Bendor, D., and Wang, X. (2007). Differential neural coding of acoustic flutter within primate auditory cortex. Nat. Neurosci. *10*, 763–771.

Bendor, D., and Wang, X. (2008). Neural response properties of primary, rostral, and rostrotemporal core fields in the auditory cortex of marmoset monkeys. J. Neurophysiol. *100*, 888–906.

Chorev, E., Epsztein, J., Houweling, A.R., Lee, A.K., and Brecht, M. (2009). Electrophysiological recordings from behaving animals—going beyond spikes. Curr. Opin. Neurobiol. *19*, 513–519.

Creutzfeldt, O., Hellweg, F.C., and Schreiner, C. (1980). Thalamocortical transformation of responses to complex auditory stimuli. Exp. Brain Res. *39*, 87–104.

de la Mothe, L.A., Blumell, S., Kajikawa, Y., and Hackett, T.A. (2006). Cortical connections of the auditory cortex in marmoset monkeys: core and medial belt regions. J. Comp. Neurol. *496*, 27–71.

Dong, C., Qin, L., Liu, Y., Zhang, X., and Sato, Y. (2011). Neural responses in the primary auditory cortex of freely behaving cats while discriminating fast and slow click-trains. PLoS ONE *6*, e25895.

Gao, X., and Wehr, M. (2015). A coding transformation for temporally structured sounds within auditory cortical neurons. Neuron *86*, 292–303.

Gao, L., Meng, X., Ye, C., Zhang, H., Liu, C., Dan, Y., Poo, M.M., He, J., and Zhang, X. (2009). Entrainment of slow oscillations of auditory thalamic neurons by repetitive sound stimuli. J. Neurosci. *29*, 6013–6021.

Heil, P. (1997). Auditory cortical onset responses revisited. II. Response strength. J. Neurophysiol. *77*, 2642–2660.

Jagadeesh, B., Wheat, H.S., Kontsevich, L.L., Tyler, C.W., and Ferster, D. (1997). Direction selectivity of synaptic potentials in simple cells of the cat visual cortex. J. Neurophysiol. *78*, 2772–2789.

Joris, P.X., Schreiner, C.E., and Rees, A. (2004). Neural processing of amplitude-modulated sounds. Physiol. Rev. *84*, 541–577.

Kleppe, I.C., and Robinson, H.P. (1999). Determining the activation time course of synaptic AMPA receptors from openings of colocalized NMDA receptors. Biophys. J. *77*, 1418–1427.

Liang, L., Lu, T., and Wang, X. (2002). Neural representations of sinusoidal amplitude and frequency modulations in the primary auditory cortex of awake primates. J. Neurophysiol. *87*, 2237–2261.

Long, M.A., and Lee, A.K. (2012). Intracellular recording in behaving animals. Curr. Opin. Neurobiol. *22*, 34–44.

Lu, T., and Wang, X. (2000). Temporal discharge patterns evoked by rapid sequences of wide- and narrowband clicks in the primary auditory cortex of cat. J. Neurophysiol. *84*, 236–246.

Lu, T., Liang, L., and Wang, X. (2001a). Neural representations of temporally asymmetric stimuli in the auditory cortex of awake primates. J. Neurophysiol. *85*, 2364–2380.

Lu, T., Liang, L., and Wang, X. (2001b). Temporal and rate representations of time-varying signals in the auditory cortex of awake primates. Nat. Neurosci. *4*, 1131–1138.

Mardia, K.V., and Jupp, P.E. (2000). Directional Statistics (John Wiley & Sons).

McCormick, D.A., Shu, Y., Hasenstaub, A., Sanchez-Vives, M., Badoual, M., and Bal, T. (2003). Persistent cortical activity: mechanisms of generation and effects on neuronal excitability. Cereb. Cortex *13*, 1219–1231.

Mickey, B.J., and Middlebrooks, J.C. (2003). Representation of auditory space by cortical neurons in awake cats. J. Neurosci. *23*, 8649–8663.

Miller, C.T., Freiwald, W.A., Leopold, D.A., Mitchell, J.F., Silva, A.C., and Wang, X. (2016). Marmosets: a neuroscientific model of human social behavior. Neuron *90*, 219–233.

Montemurro, M.A., Rasch, M.J., Murayama, Y., Logothetis, N.K., and Panzeri, S. (2008). Phase-of-firing coding of natural visual stimuli in primary visual cortex. Curr. Biol. *18*, 375–380.

Moore, B.C. (2003). An Introduction of the Psychology of Hearing (Academic).

Osmanski, M.S., and Wang, X. (2011). Measurement of absolute auditory thresholds in the common marmoset (Callithrix jacchus). Hear. Res. *277*, 127–133.

Peretz, I., and Zatorre, R.J. (2005). Brain organization for music processing. Annu. Rev. Psychol. *56*, 89–114.

Phillips, D.P. (1985). Temporal response features of cat auditory cortex neurons contributing to sensitivity to tones delivered in the presence of continuous noise. Hear. Res. *19*, 253–268.

Priebe, N.J., Mechler, F., Carandini, M., and Ferster, D. (2004). The contribution of spike threshold to the dichotomy of cortical simple and complex cells. Nat. Neurosci. *7*, 1113–1122.

Rabang, C.F., and Bartlett, E.L. (2011). A computational model of cellular mechanisms of temporal coding in the medial geniculate body (MGB). PLoS ONE *6*, e29375.

Romo, R., and Salinas, E. (2003). Flutter discrimination: neural codes, perception, memory and decision making. Nat. Rev. Neurosci. *4*, 203–218.

Rosen, S. (1992). Temporal information in speech: acoustic, auditory and linguistic aspects. Philos. Trans. R. Soc. Lond. B Biol. Sci. *336*, 367–373.

Sadagopan, S., and Wang, X. (2008). Level invariant representation of sounds by populations of neurons in primary auditory cortex. J. Neurosci. *28*, 3415–3426.

Salinas, E., Hernandez, A., Zainos, A., and Romo, R. (2000). Periodicity and firing rate as candidate neural codes for the frequency of vibrotactile stimuli. J. Neurosci. *20*, 5503–5515.

Singh, N.C., and Theunissen, F.E. (2003). Modulation spectra of natural sounds and ethological theories of auditory processing. J. Acoust. Soc. Am. *114*, 3394–3411.

Song, X., Osmanski, M.S., Guo, Y., and Wang, X. (2016). Complex pitch perception mechanisms are shared by humans and a New World monkey. Proc. Natl. Acad. Sci. USA *113*, 781–786.

Steriade, M., Nuñez, A., and Amzica, F. (1993). A novel slow (< 1 Hz) oscillation of neocortical neurons in vivo: depolarizing and hyperpolarizing components. J. Neurosci. *13*, 3252–3265.

Tan, A.Y., Chen, Y., Scholl, B., Seidemann, E., and Priebe, N.J. (2014). Sensory stimulation shifts visual cortex from synchronous to asynchronous states. Nature *509*, 226–229.

Wang, X. (2000). On cortical coding of vocal communication sounds in primates. Proc. Natl. Acad. Sci. USA *97*, 11843–11849.

Wang, X. (2007). Neural coding strategies in auditory cortex. Hear. Res. *229*, 81–93.

Wang, X., Lu, T., Snider, R.K., and Liang, L. (2005). Sustained firing in auditory cortex evoked by preferred stimuli. Nature *435*, 341–346.

Wang, X., Lu, T., Bendor, D., and Bartlett, E. (2008). Neural coding of temporal information in auditory thalamus and cortex. Neuroscience *157*, 484–494.

Zanos, T.P., Mineault, P.J., and Pack, C.C. (2011). Removal of spurious correlations between spikes and local field potentials. J. Neurophysiol. *105*, 474–486.